# FLUID MECHANICS SIMULATION OF 3D-PRINTED SCAFFOLDS IN A BIOREACTOR SYSTEM

A Honors Thesis Presented in Partial Fulfillment of the Requirements for Graduation with Honors Research Distinction in the Department of Biomedical Engineering at

The Ohio State University

Nguyen “Archie” Tram

Spring 2016

| Defense Committee Member | Approval |
| --- | --- |
| Samir Ghadiali, Ph.D., Advisor | _____ |
| David Dean, Ph.D., Co-advisor | _____ |

Copyright by

Nguyen Khoi Tram

2016

**ABSTRACT**

Perfusion of porous scaffolds may enhance osteogenesis through increased mass transport and shear stress stimulation. Therefore, it is important to quantify the fluid mechanics, especially the fluid-induced shear stresses, present in the perfusion bioreactor systems used to culture scaffolds. Experimental measurement of shear stress is improbable since there is no practical method available to measure the shear stress distribution on the surface of a complex three-dimensional scaffold. This study aims to computationally simulate fluid flow in a bioreactor and to correlate the estimated shear stress with biological outcomes. Specifically, scaffold models with a Schoen's gyroid pore geometry were generated using MATLAB. The COMSOL Multiphysics software package was used to solve the governing fluid-dynamic equations (Navier-Stokes). The computer simulations identified a significant shortcoming of the bioreactor system; appropriate changes were made to fix the problem. A simple yet useful equation was derived to convert flow rates used in published literature on perfusion systems to shear stresses that cells would experience on the surfaces of the scaffolds. The combination of computer simulations with experimental studies on the effect of flow will accelerate our progress in making effective scaffolds for bone tissue engineering applications.

**ACKNOWLEDGEMENT**

First and foremost, I would like to thank my thesis advisors, Dr. Samir Ghadiali and Dr. David Dean, for all of their advice and leadership throughout my work on this thesis project. I would also like to thank my direct supervisors, Dr. Jason Walker and Alison Claybon, for their constant supports and motivations that encouraged me to go beyond my limit, in addition to many enjoyable conversations concerning both work and life. Additionally, I would like to thank my laboratory peers who made my research project possible: Ryan Sefcik and Briana Swan, for their assistance in cell culturing; Rachel Zielinski, for her assistance in computer simulations; Tyler Meder, for his assistance in building the perfusion bioreactor system; Daniel Cleveland, for his initial work on the bioreactor illustration; and the rest of the Osteo Engineering Laboratory, who have made work fun and have become an irreplaceable part of my undergraduate career at The Ohio State University.

This work was supported by the Army, Navy, NIH, Air Force, VA and Health Affairs to support the AFIRM II effort, under Award No. W81XWH-14-2-0004. The U.S. Army Medical Research Acquisition Activity, 820 Chandler Street, Fort Detrick MD 21702-5014 is the awarding and administering acquisition office. Opinions, interpretations, conclusions and recommendations are those of the author and are not necessarily endorsed by the Department of Defense.

**TABLE OF CONTENTS**

**LIST OF FIGURES**

## LIST OF TABLES

# CHAPTER 1: INTRODUCTION

One of the goals of tissue engineering is to restore the function of damaged tissues due to aging, accidents, or diseases. Bone tissue engineering (BTE), in particular, has the potential to overcome the disadvantages of current "gold-standard" bone replacing procedures such as autografts or allografts. A dominant method of BTE involves culturing cells on biocompatible structures (scaffolds) *in vitro* to form artificial bone constructs (Langer et al., 1993). Additive manufacturing, colloquially known as three-dimensional (3D) printing, provides a versatile and replicable platform to fabricate scaffolds, as shown in Figure 1 (Atala et al., 2015). With the use of digital light printing (DLP) technology, poly(propylene fumarate) (PPF) has been utilized as a biocompatible and resorbable printing material for BTE (Luo et al., 2016; Dean et al., 2003; Lee et al., 2011; Temenoff et al., 2000; Wang et al., 2006; Fisher et al., 2002).

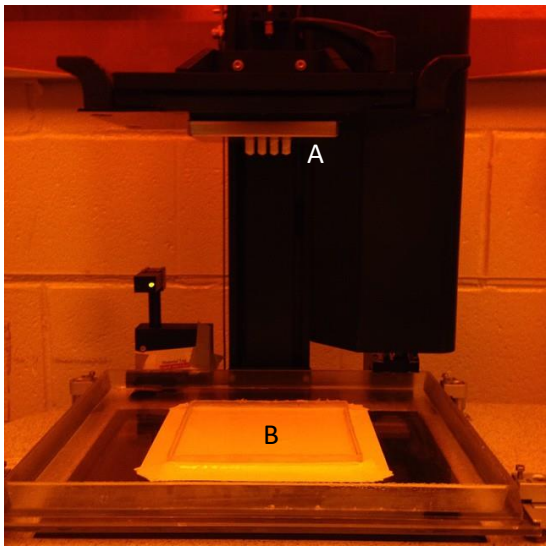


Figure 1: 3D printed scaffolds (A) photo-crosslinked from a pool of liquid polymer resin (B).

Porosity is a critical characteristic of a scaffold as it affects a scaffold's mechanical integrity, in vivo resorption profile, and surface area for cell attachment, proliferation and differentiation.

Scaffolds with Schoen's Gyroid triply periodic minimal surface (TPMS) pore architecture mimic the macrostructures from some living organisms (Michielsen et al., 2008) and might provide a preferable environment for wound healing and development of cells (Figure 2). Moreover, since the TPMS surfaces are mathematically defined, the scaffolds with Gyroid-based porosity can be tailored to have specific porosity, pore size, or strut size. Remarkably, many scaffolds in other studies have been created using techniques that are not readily replicable (Ratner et al., 2004; Maes et al., 2009; Maes et al., 2012). For techniques such as salt leaching or foaming, the pore-forming reagents are randomized spatially; as a result, the scaffolds generated are not identical to each other. Other groups used scaffolds with irregular architecture derived from trabecular bone, which is prone to a nonhomogeneous flow profile where a majority of fluid goes through only one or two openings, leaving a large portion of the scaffold with stagnant fluid (Grayson et al., 2010; Grayson et al., 2011; Liu et al., 2013; Cartmell et al., 2003). In contrast, computer-generated gyroid scaffolds can be repeatedly made with interconnected pores, ensuring a homogenous flow that provides even distribution of nutrients to cells in the scaffolds.

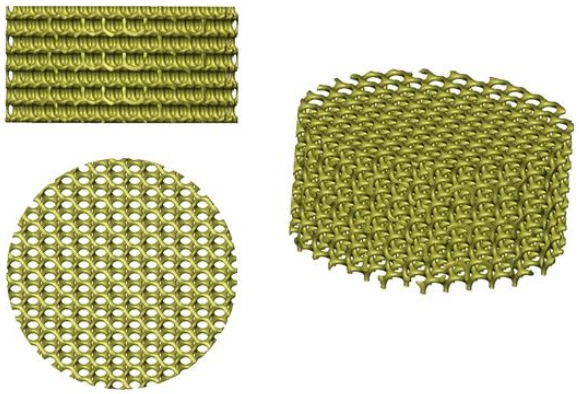

Figure 2: CAD models of a scaffold with Schoen's Gyroid TPMS pore architecture.

A major hurdle in BTE has been forming fully-viable bone grafts for greater-than-critical size defects, which are several centimeters in size. A large 3D construct (> 1 $cm^3$) in static culture often

has a dense layer of cells at the construct's periphery, while cells within the core regions are less active or even necrotic (Ishaug et al., 1997; Ishaug-Riley et al., 1998; Holy et al., 2000). This nutrient supply problem is typically found in *in vitro* static culture, where the cellular consumption rate exceeds the diffusion of nutrients due to the absence of a vascular blood supply commonly found *in vivo*. Dynamic *in vitro* culture, through the use of perfusion bioreactors, overcomes the "size barrier" by inducing a flow that penetrates the interior of the scaffold. By providing a convective transfer of nutrients and oxygen, perfusion bioreactors may eliminate the problems associated with static nutrient diffusion limit; additionally, dynamic culture enables the application of physical stimulation to cells. Consequently, the use of bioreactors with culture medium flow has been commonly proposed as a means to improve 3D bio-constructs for tissue engineering (Liu et al., 2013; Wang et al., 2010; Martins et al., 2010; Mahmoudifa et al., 2010; Grayson et al., 2008; Grayson et al., 2010; Martin et al., 2010; Goldstein et al., 2001; Marolt et al., 2006; Meinel et al., 2004; Sikavitsas et al., 2002; Bancroft et al., 2002; Glowacki et al., 1998).

Besides providing improved chemotransport, perfusion bioreactors also create fluid-induced shear stress which has been found to influence the development of cells (Korin et al., 2007; Cartmell et al., 2003; Liu et al., 2013; Grayson et al., 2011). For example, a shear stress of 10 mPa was reported to significantly improve cell proliferation and align fibroblasts along the flow direction *in vitro* (Korin et al., 2007). In contrast, a shear stress of 20 mPa or above could detach cells on the surface of a scaffold, as reported in (Liu et al., 2013). Therefore, it is important to quantitatively assess the fluid-induced shear stress present in the perfusion bioreactor systems that are used to culture scaffolds. Experimental measurement of shear stress on the surface of a 3D scaffold is improbable. While micro-particle-image velocimetry could be used to measure the fluid-induced strain rate on the surface of cells (Song et al., 2013), this method is limited to only 2D constructs, hence, cannot

be used to measure shear stresses on the surfaces of complex 3D scaffolds. Computational fluid dynamics (CFD) is a technique that could provide an estimation of shear stress on the surface of a scaffold. Past computer simulation studies of shear stress have been focused on irregular scaffolds (Maes et al., 2009; Maes et al., 2012; Grayson et al., 2010; Cioffi et al., 2006; Jungreuthmayer et al., 2009); to the author's knowledge, fluid dynamic characteristics of scaffolds with gyroid pore architecture have not been studied.

In this study, we investigated the shear stress distributions of gyroid scaffolds in the perfusion bioreactors using the CFD method. Another goal of the CFD models was to detect any potential shortcomings in the bioreactor set up and provide flow rates that would induce desirable shear stresses on the scaffolds. A finite element model capable of determining fluid-induced shear stress on a scaffold's surface was created *in silico*. To validate the shear stress obtained from the computer simulations, a simple engineering model of the porous scaffold with an analytical solution for surface shear stress was created; additionally, a meta-analysis was conducted to approximate shear stress from flow rates used in previously published perfusion studies. Through the use of computer simulations, a fault in the bioreactor system was identified and addressed. Based on the *in silico* results, we designed a biological laboratory experiment to investigate how changes in shear stress, induced from varying bioreactor inlet velocities, alter cellular behavior. The ability to manipulate the shear stresses present on a scaffold is an important step in controlling the behavior and growth of cells within the scaffold.

# CHAPTER 2: MATERIALS AND METHODS

## 2.1 Mathematical Model for Wall Shear Stress on the Scaffolds in a Perfusion System

A simple mathematical equation was derived to determine the average shear stress imparted to the scaffold's surface from the flow rates used in the previously published literature on perfusion systems. The complete derivation is shown in Appendix A. The porosity of the bone scaffolds was modeled as a bundle of hollow cylinders arranged longitudinally, parallel to the perfusion direction, as described by Grayson et al. (2008). The shear stress equation was given by:

$$\tau = \frac{4 \times \mu \times Q}{d_p \times \pi R^2}$$

where $\tau$ is the wall shear stress, $\mu$ is the viscosity of the medium, $Q$ is the volumetric flow rate, $d_p$ is the diameter of the pore, and R is the radius of the cylindrical scaffold.

## 2.2 Computer Simulations

### 2.2.1 Creating and Refining the Computer-Assisted-Design (CAD) Scaffold Models

Scaffold models with Schoen's Gyroid-type Triply Periodic Minimal Surface pore architecture were made using MATLAB (The MathWorks, Inc., Natick, MA). The scaffold's strut size is 0.2 mm and its pore size is 0.7 mm. The first CAD model was a cylindrical scaffold with a height of 1 mm and a diameter of 2 mm (D2 – H1); the second model had a similar geometry but with a height of 10 mm and a diameter of 10 mm (D10 – H10). The final model was also cylindrical but with a height of 4 mm and diameter of 8 mm (D8 – H4); additionally, the third model was divided into quarters longitudinally and only one quadrant was analyzed. These CAD models were saved as stereolithography (STL) files, which compose of triangles (in the order of a couple million) that describe the geometry of the scaffold. The numbers of triangles on the STL files were reduced to

12,000 and the triangles' arrangements were decimated and regularly remeshed using AMIRA (FEI, Hillsboro, OR). Self-intersecting faces, holes, and non-manifold surfaces were repaired using MESHLAB (open source software, sourceforge.net). The STL file containing the surfaces of the scaffolds were converted to solid IGES format using Rhinoceros (McNeel North America, Seattle, WA), for CFD analysis.

### 2.2.2 Computational Fluid Dynamics Analysis

COMSOL Multiphysics Modeling Software (COMSOL, Inc. Burlington, MA) was used for CFD analysis of the scaffold. The scaffolds were put in the center of the scaffold chamber, which is a cylinder with a diameter of 11.9 mm for the first and second models and 8.6 mm for the third model. A unidirectional flow was perfused through the bioreactor chamber in the longitudinal direction. The perfusing fluid was defined as water, a Newtonian and incompressible fluid, with a density of 1000 kg/m$^3$ and dynamic viscosity of 1.0093 mPa·s; The Reynolds number can be calculated using this equation:

$$Re = \frac{\rho \cdot u \cdot d_p}{\mu}$$

Where $Re$ is the Reynolds number, $\rho$ is the fluid density, u is the fluid velocity, $d_p$ is the pore diameter, and μ is the fluid dynamic viscosity. The maximum Reynolds number was calculated by using the maximum local flow velocity, obtained from the computer simulations, of 0.857 m/s, and the scaffold pore diameter of 0.7 mm. The calculated Reynolds number is 594, suggesting that the flow can be assumed as laminar.

The governing Navier-Stokes equations that describe the laminar flow were given by:

$$\underbrace{0}_{a} = \underbrace{-\nabla p}_{b} + \underbrace{\nabla \cdot [\mu(\nabla u + (\nabla u)^T)]}_{c} + \underbrace{F}_{d} \qquad (1)$$

$$\rho \nabla \cdot (u) = 0 \quad (2)$$

Where $u$ is the fluid velocity, $p$ is the fluid pressure, $\rho$ is the fluid density, and μ is the fluid dynamic viscosity. The different terms in equation (1) (labeled alphabetically) correspond to the ignored inertial forces (a), pressure forces (b), viscous forces (c), and the external forces (e.g. gravitation) applied to the fluid (d). The governing Navier-Stokes equations (1) are solved with the continuity equation (2), which represents the conservation of mass as the incompressible fluid is being perfused through the bioreactor chamber.

A pair of velocity-pressure boundary conditions was used to solve the governing Navier-Stokes equation. To obtain the target median shear stresses of 0.025, 0.25, 2.5, and 25 mPa, inlet velocities of 3.57, 35.71, 357.14, or 3571.43 μm/s were assigned to the bottom surface of the bioreactor chamber, respectively, while a pressure outlet of 0 Pa was assigned to the top of the chamber (Figure 3). Both inlet and outlet were assumed to have an entrance length of 1 m. No slip boundary condition was assigned to the bioreactor walls and scaffold's surface. To study the effects of oscillatory flow on the shear stress distribution of the scaffold, negative flow rates were assigned to the inlet.

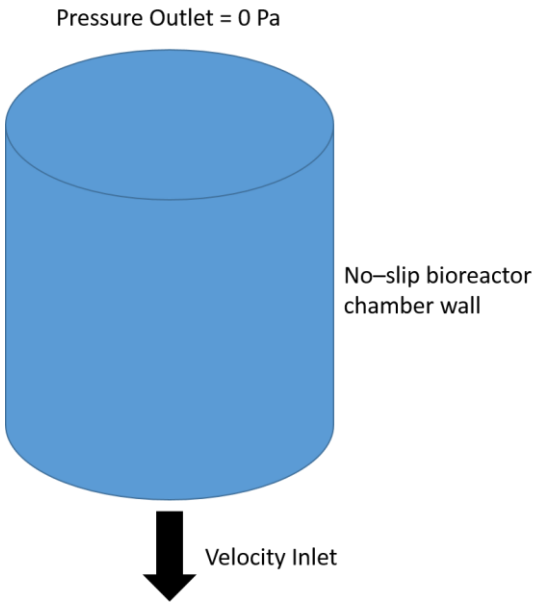


Figure 3: Schematic of the boundary conditions of the CFD models

### 2.2.3 Exploratory CFD Studies

#### 2.2.3.1 Scaffold Height Study

The D10 – H10 scaffold model (Figure 4) was divided into quarters and reduced in height to 1.5 mm, 2 mm, or 3 mm. Within the computational power at-hand, it was impossible to analyze large structures (with inherently more elements) without compromising resolution beyond reason. As a result, studying scaffolds with heights larger than 3 mm was technically challenging.

#### 2.2.3.2 Non-Perfusing Flow Study

A scaffold model with a diameter of 10 mm and a height of 10 mm (D10 – H10) was made; its pore size was 0.7 mm and its strut size was 0.2 mm. The diameter of the perfusion chamber was 11.9 mm. A particle trace plot showing the fluid movement from the inlet was generated using ADINA (ADINA R & D Inc., Watertown, MA).

The effect of decreasing the gap between scaffold and bioreactor chamber on shear stress distribution was studied in a scaffold diameter study. Specifically, scaffold models of height 2 mm with diameters 10 mm, 10.49 mm, or 10.8 mm were made; only a quarter of the scaffold was analyzed. It was technically challenging to make scaffolds with a diameter larger than 10.8 mm.

#### 2.2.3.3 Scaffold Pore Size/ Strut Size Study

A small scaffold model with a diameter of 2 mm and a height of 1 mm (H1 – D2) was made to improve computation efficiency. The strut size of the scaffold varied from 0.125 mm to 0.3 mm and the pore size varied from 0.3 to 0.7 mm. Average shear stress on the surface of each scaffold model was reported.

### 2.2.4 Reduction of the CAD model

Since the struts of the scaffold were very small (0.2 mm) compared to the overall size of the cylindrical scaffold (height and diameter up to 10 mm), COMSOL needed to have at least 1 million tetrahedral elements to appropriately describe the geometry of the whole scaffold. Subsequently, millions of degrees of freedom (DOF) were needed to solve the CFD model, requiring more than 100 gigabytes of random-access memory. Due to limitations in computing power, CAD models of the scaffold must be reduced to a more manageable size so the models can be efficiently solved. Since the D8 – H4 CAD model was symmetrical in the sagittal planes, the cylindrical scaffold was divided into quarters longitudinally. Subsequently, one quadrant of the scaffold was meshed and studied; symmetry boundary condition was assigned to the newly cut surfaces in the CAD model.

### 2.2.5 Flow Development Study

Although the inlet and outlet were both assigned an entrance length of 1 m before coming into the region of interest (ROI) which composes of the D8 – H4 scaffold and the surrounding fluid, a

reasonable distance between the inlet/outlet to the scaffold is required for fully-developed flow to adjust to the presence of the scaffold without forcing the fluid through highly preferential flow paths (Figure 4). Although leaving ample room for the flow to develop inside the ROI is generally a good idea, it would generally require more computing power as well. In this study, entrance lengths of 0 mm, 8 mm, 16 mm, 24 mm, and 32 mm (for both inlet and outlet) were compared in the scaffold chamber model.

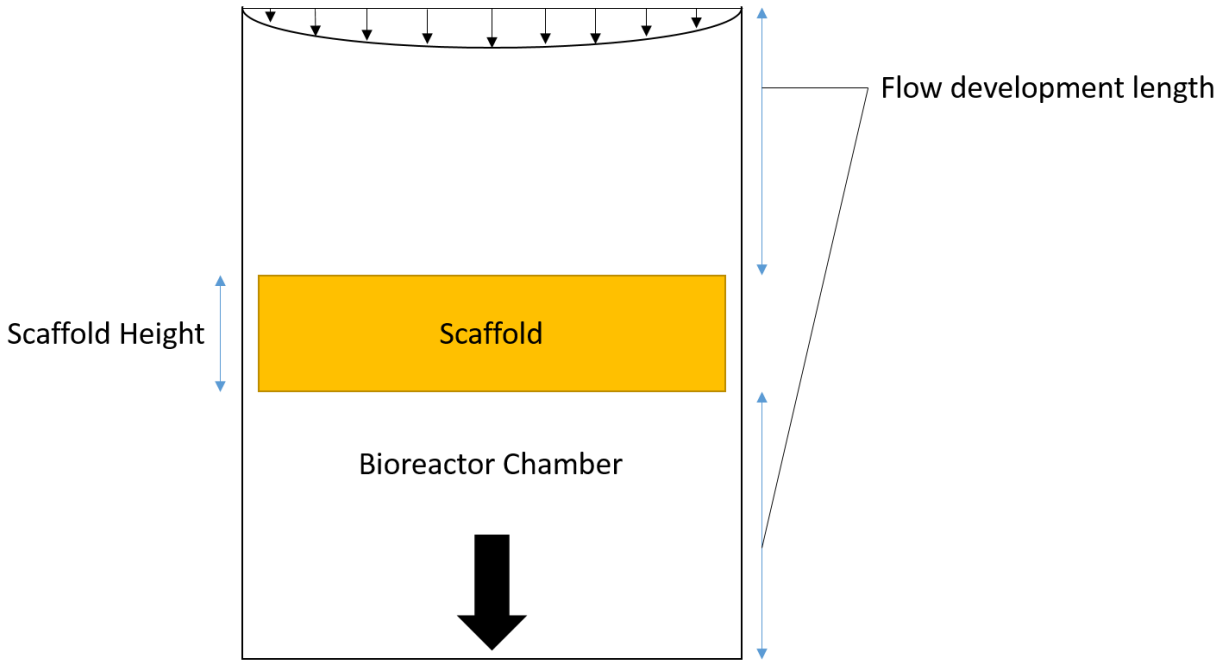


Figure 4: Schematic of the flow development study.

### 2.2.6 Mesh Convergence Study

An appropriate amount of elements must be created to correctly approximate the results without taking too much computing power or time. D8 – H4 scaffold models with increasing mesh densities (from "Extra Coarse" to "Normal" as prescribed in COMSOL) were created and run with identical

boundary conditions. When significant changes in the mesh density resulted in insignificant experimental results, the mesh density was characterized as appropriate.

### 2.2.7 Post Analysis of CFD Models

Shear stress at each point on the discretized surface was obtained, using this equation:

$$\tau = \mu \times \dot{\gamma}$$

Where $\tau$ is the datum's shear stress, $\mu$ is dynamic viscosity, and $\dot{\gamma}$ is the datum's shear rate. The text data were imported into MATLAB. Since the distribution of the shear stresses is not normal (the distribution failed the Kolmogorov–Smirnov test), the median shear stress values were used to calculate the percent differences between each model. Specifically, the median stress value of the "best" model (e.g. highest density mesh or longest flow development length) was compared to the values of the subsequent models. Percent difference was calculated for each comparison using this equation:

$$\%\, difference = \frac{\Delta median * 100}{median\ of\ the\ "best"\ model} \quad (3)$$

Normally, a percentage difference of 5% or below is considered insignificant. Due to limitation in computation power, a more relaxed criterion was required. As a result, a percentage difference of 10% or below was considered to be a good approximation to the correct value.

## 2.3 Experimental Bioreactor Study

### 2.3.1 Additive Manufacturing of Poly (Propylene Fumarate) Scaffolds

Poly(propylene fumarate) (PPF) scaffolds were three-dimensionally (3D) printed using an EnvisionTEC Pecfactory 3 DDP 3D printer (EnvisionTEC, Inc., Dearborn, MI) as detailed in Luo 2016. The printer was calibrated to generate an ultraviolet (UV) mask with a nominal irradiance

of 350 mW $dm^{-2}$. UV light projected from the printer initiates the crosslinking process of PPF, forming a solid structure from the liquid resin. The printed scaffolds have a diameter of 8 mm, height of 4 mm, struts of 0.2 mm, and pores of 0.7 mm. Once 3D printed, the scaffolds were briefly rinsed three times with acetone, ethanol, and distilled water to remove any uncured resin from within the pores of the scaffolds. The scaffolds were placed in a ProCure 350 UV Chamber (3D Systems, Valencia, CA) for 8 hours to complete further cross-linking.

Table 1: The scaffold washing process

| Step | Solution | Time (minutes) |
|---|---|---|
| 1 | Phosphate-buffered saline | 5 |
| 2 | 49% ethanol, 21% acetone, and 30% distilled water | 25 |
| 3 | Phosphate-buffered saline | 5 |
| 4 | Phosphate-buffered saline | 5 |
| 5 | Phosphate-buffered saline | 5 |
| 6 | 49% ethanol, 21% acetone, and 30% distilled water | 15 |
| 7 | Phosphate-buffered saline | 5 |
| 8 | Phosphate-buffered saline | 5 |
| 9 | Phosphate-buffered saline | 5 |

The scaffolds were thoroughly washed as detailed in Table 1. Each solution was added to fully submerge the scaffolds then aspirated. The washed scaffolds were submerged in fresh phosphate-buffered saline, covered with aluminum foil, and sterilized in a Getinge 6610 autoclave (Getinge Sterilization AB, Sweden) using the liquid cycle (P3 – Liquids). After sterilization, the scaffolds were soaked in fetal bovine serum overnight.

### 2.3.2 L929 Mouse Fibroblasts

Mouse L929 fibroblasts were cultured at 37 $^{o}$C and 95% air/ 5% carbon dioxide in a HERAcell 150i CO2 incubator (Thermo Fisher Scientific) using Dulbecco's Modified Eagle Medium (DMEM) supplemented with 10% fetal bovine serum (FBS) and 1% Penicillin Streptomycin (Pen-Strep). The cells were grown to confluent, as observed with a Nikon Diaphot TMD (Nikon Corp., Japan) microscope, in T-75 flasks before seeded on scaffolds with a cell density of 1000 cells/mm$^2$. Since the surface area of the scaffold is 600 mm$^2$, the total number of cells used was 600,000 cells per scaffold. Complete DMEM medium (0.8 ml) and cell suspension (42.55 µl) were added to each well containing the scaffold in a 24-well plate. A vacuum chamber was used to eliminate air bubbles inside the pores of the scaffolds. The cells were allowed to attach to the surface of the scaffolds for 5 hours before the scaffolds were transferred into the bioreactor chambers. Scaffolds in dynamic culturing conditions (n = 5 for each flow rate) were perfused in the bioreactor chambers for 4 days. As positive controls, scaffolds (n = 5) was simultaneously cultured in static condition. All groups (static and dynamic culturing conditions) have a scaffold with no seeded cells, which acted as negative controls. Additionally, cell-seeded scaffolds (n = 5) were analyzed at time 0 to evaluate the seeding efficiency. MTT cell proliferation assay, which works based on the reduction of tetrazolium salt in the presence of metabolically active cells, was our choice to quantify cellular proliferation.

### 2.3.3 Bioreactor System

#### 2.3.3.1 Assembling

The three main components of the bioreactor system are syringe pumps, scaffold chambers, and media reservoirs (Figure 5). The reservoirs (one-liter Erlenmeyer flasks), which are placed in the

incubator, contain the culture medium to be perfused through the scaffolds. Scaffold chambers, which are inside the incubator and contain the scaffolds, are 3-ml syringes (BD 3 ml Syringe with Luer-Lok Tip) with the plungers removed. Syringe pumps (Harvard Apparatus, Holliston, MA) act as the power source outside the incubator that drives the culture medium from the reservoirs, through the scaffold chambers, into 60-ml syringes (Monoject 60-ml syringe with Luer-Lok tip) connected at the pumps. The components are connected using gas-permeable PDMS tubing (Cole-Parmer C-FLEX tubing 06422-02) with Luer locks and pinch clamps (obtained from QOSINA).

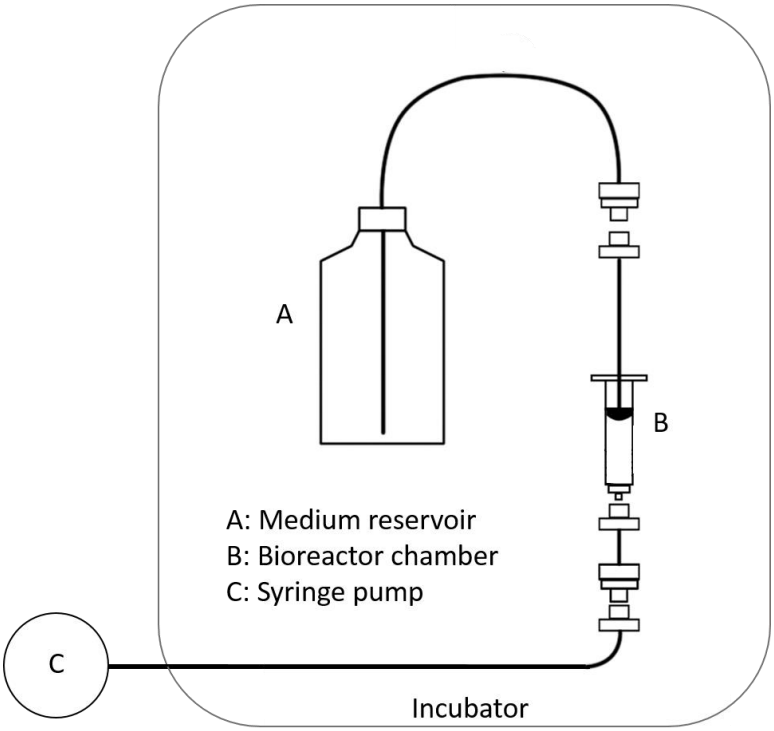


Figure 5: Schematic of the perfusion system

### 2.3.3.2 Priming the Perfusion System and Placing the Scaffolds

The bioreactor system was primed in a Biosafety Cabinet (NUAIRE Class II Type A2) before and then placed into an incubator. Specifically, a 60-ml syringe was used to push cell medium upward through the scaffold chambers into the reservoirs. After priming, tubing at the two ends of the

scaffold chambers was clipped and plug gaskets were removed from the chambers. The cell-seeded scaffolds were carefully placed in the bottom of the chambers. Extra culture medium was added before the gaskets were inserted into the chambers to ensure a primed culture environment with minimal air bubbles. Detailed instructions for assembling, priming, and placing the scaffolds are given in Appendix B. For ease in keeping a primed and sterile bioreactor system, the lines outside of the incubator were only primed once all lines were connected and clamps were unclipped.

#### 2.3.3.3 Flow Configurations

The scaffolds (n = 5 for each flow rate) were perfused for 4 days in an oscillatory mode with volumetric flow rates of 0.76, 7.57, 75.73, and 757.30 ml/hour to obtain the target medium shear stresses of 0.025, 0.25, 2.5, and 25 mPa, respectively (Table 2). The first refilling step was to prime the lines outside the incubator and to remove any remaining air bubbles within the system. The incubator was set at 37 $^{o}$C with 95% air/ 5% carbon dioxide.

Table 2: The configuration of the syringe pump in an oscillatory mode.

| Step | Action |
|---|---|
| 1 | Refill 10 ml with the desired flow rate |
| 2 | Refill 40 ml with the desired flow rate |
| 3 | Infill 40 ml with the desired flow rate |
| 4 | Repeat from step 2 |

# CHAPTER 3: RESULTS AND DISCUSSIONS

## 3.1 Meta-analysis of Published Literature

A simple mathematical equation was derived to determine the average shear stress on the surface of the scaffold using information (e.g. volumetric flow rate, pore diameter, and construct radius) provided in the perfusion literature. The average shear stresses on the D8 – H4 scaffold induced from different flow rates were also calculated using this engineering model. The findings were summarized in Table 3. Any shear stress values reported in the published articles were also included for comparison. Except for the shear stress value reported in Sandino et al. 2008 and one of the values reported in Jungreuthmayer et al. 2009, the calculated and simulated shear stresses are generally in the same magnitude, supporting the validity of this mathematical model.

This mathematical equation was used to determine the unreported shear stresses from past publications, using the given flow rates. Cellular behaviors at each flow rate were included to correlate the effects of shear stress on cells. All data were compiled in Table 4. Shear stresses were arranged in increasing order to show the spectrum of how shear stress affects cellular behaviors.

Table 3: Calculations of average shear stresses from the published literature.

| Reference | Pore size (mm) | Construct radius (mm) | Flow rate (mm3/s) | Calculated SS (mPa) | Simulated SS (mPa) |
|---|---|---|---|---|---|
| Sandino et al. 2008 | 0.350 | 0.500 | 0.008 | 0.229 | 37.000 |
| Jungreuthmayer et al. 2009 | 0.350 | 2.500 | 1056.361 | 1229.714 | 7500.000 |
| Jungreuthmayer et al. 2009 | 0.096 | 0.320 | 0.076 | 19.583 | 200.000 |
| Cioffi et al. 2006 | 0.100 | 0.200 | 0.007 | 4.240 | 3.280 |
| Cioffi et al. 2006 | 0.100 | 0.200 | 0.001 | 0.916 | 2.560 |
| Cioffi et al. 2006 | 0.100 | 0.200 | 0.014 | 9.160 | 25.600 |
| Maes et al. 2009 | 0.270 | 0.500 | 0.027 | 1.007 | 1.400 |
| Maes et al. 2009 | 0.270 | 0.750 | 0.060 | 1.007 | 1.950 |
| Maes et al. 2009 | 0.280 | 0.500 | 0.027 | 0.971 | 1.100 |
| Maes et al. 2009 | 0.280 | 0.750 | 0.060 | 0.971 | 1.460 |
| Maes et al. 2012 | 0.270 | 2.500 | 0.668 | 1.007 | 1.410 |
| Maes et al. 2012 | 0.280 | 2.500 | 0.668 | 0.971 | 1.090 |
| This study | 0.700 | 4.000 | 0.118 | 0.027 | 0.014 |
| This study | 0.700 | 4.000 | 1.178 | 0.270 | 0.140 |
| This study | 0.700 | 4.000 | 11.780 | 2.703 | 1.400 |

Table 4: Compilation of the effects of shear stresses on cellular behaviors.

| Reference | Shear stress (mPa) | Effect |
|---|---|---|
| Jarman-Smith et al., 2004 | 0.03 | proliferate slowly at day 4, higher at day 6 forward |
| Cartmell et al., 2003 | 0.07 | cell DNA decreases as shear stress increases |
| Cartmell et al., 2003 | 0.73 | cell DNA decreases as shear stress increases |
| Cartmell et al., 2003 | 1.46 | cell DNA decreases as shear stress increases |
| Cartmell et al., 2003 | 7.31 | cell DNA decreases as shear stress increases |
| Grayson et al., 2010 | 0.99 | "substandard results" |
| Grayson et al., 2010 | 4.93 | "best results" |
| Grayson et al., 2010 | 9.86 | "best results" |
| Grayson et al., 2010 | 14.78 | "substandard results" |
| Grayson et al., 2010 | 22.18 | "substandard results" |
| Korin et al., 2007 | 0.99 | more proliferation as shear stress increases |
| Korin et al., 2007 | 9.86 | more proliferation as shear stress increases |
| Korin et al., 2007 | 29.59 | more cells get washed out as shear stress increases |
| Korin et al., 2007 | 49.31 | more cells get washed out as shear stress increases |
| Korin et al., 2007 | 98.62 | more cells get washed out as shear stress increases |
| Liu et al., 2013 | 19.92 | more cells get washed out as shear stress increases |
| Liu et al., 2013 | 31.18 | more cells get washed out as shear stress increases |
| Liu et al., 2013 | 42.44 | more cells get washed out as shear stress increases |
| Liu et al., 2013 | 52.84 | more cells get washed out as shear stress increases |

## 3.2 Exploratory CFD Studies

### 3.2.1 Scaffold Height Study

Histograms of shear stresses on scaffolds with different heights were plotted on the same graph for comparison, as shown in Figure 7. The shapes of the histograms are not generally different from each other; however, differences between each model can still be discerned. Specifically, the scaffold with height 1.5 mm has a higher population of shear stresses ranging from 0.22 – 0.36 mPa than the other two models, while the scaffold with height 3 mm has the highest peak at the shear stress 0.1 mPa. The percent differences in median shear stresses between the models with different heights were calculated using Equation #3 and are listed in Table 5. While the differences in cases 2 and 3 are below 10%, which would qualify as insignificantly different based on the relaxed criterion, the difference in median shear stress becomes significant when there is a larger difference in the model heights, as shown in case 1. Considering the potentially significant errors in using models with reduced heights, scaffold models with full height were used in future studies.

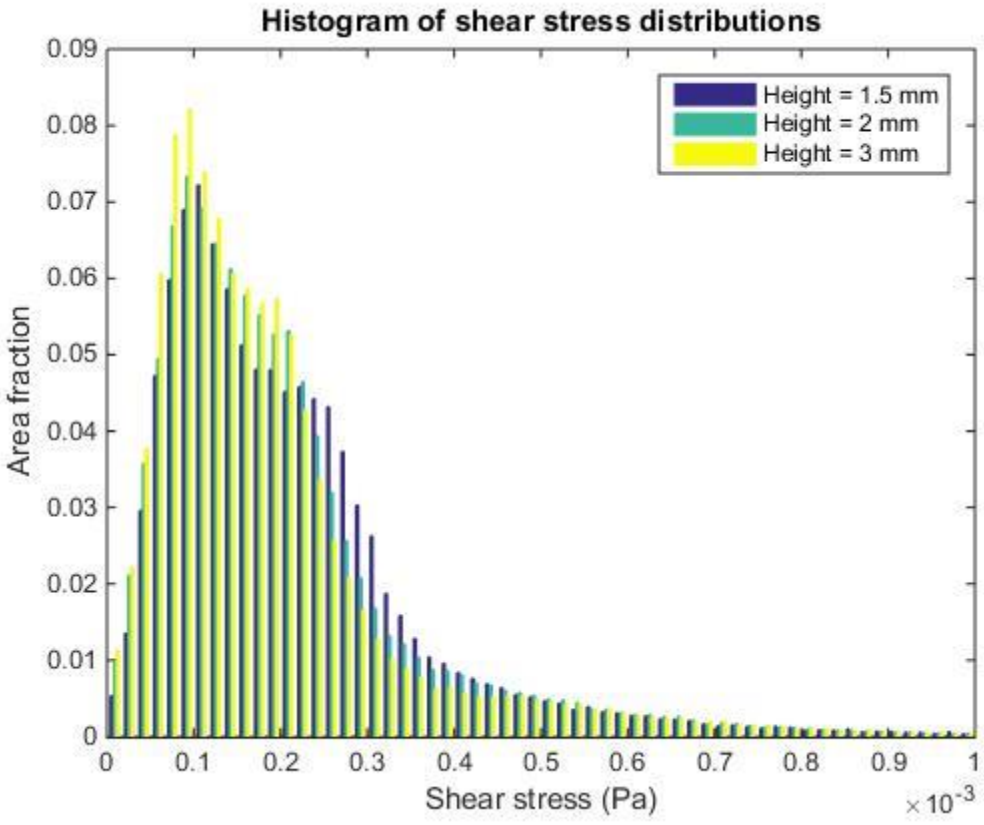


Figure 6: Shear stress distributions of scaffolds with different heights.

Table 5: Percent differences in median shear stresses of scaffolds with different heights

| Case | 1: 1.5 mm vs. 3 mm | 2: 2 mm vs. 3 mm | 3: 1.5 mm vs. 2 mm |
|---|---|---|---|
| Percent Difference | 17.2% | 8.5% | 8.0% |

### 3.2.2 Non-perfusing flow study

A particle trace plot was generated to show the movement of fluid through a bioreactor chamber of diameter 11.9 mm holding a scaffold with a diameter of 10 mm and a height of 10 mm (Figure 6). The particle trace plot shows a highly preferential pathway in the gap of 0.95 mm between the bioreactor's wall and the scaffold's outer wall. There seemed to be little to no fluid movement inside the pores of the scaffold. This issue was addressed in a technical note on a bioreactor system

(Bancroft et al., 2004) and this phenomenon was coined “non-perfusing flow”. Potential problems associated with non-perfusing flow include poor nutrient and growth factor transport and waste removal in the pores of the scaffolds as well as undesirably high shear stresses on the outer surface of the scaffold. To eliminate non-perfusing flow, the gap between the bioreactor wall and the outer layer of scaffold needs to be reduced. This study identified a previously unknown fault in our perfusion system and provided a means to ensure that medium is evenly perfused through the scaffolds in the actual experiments.

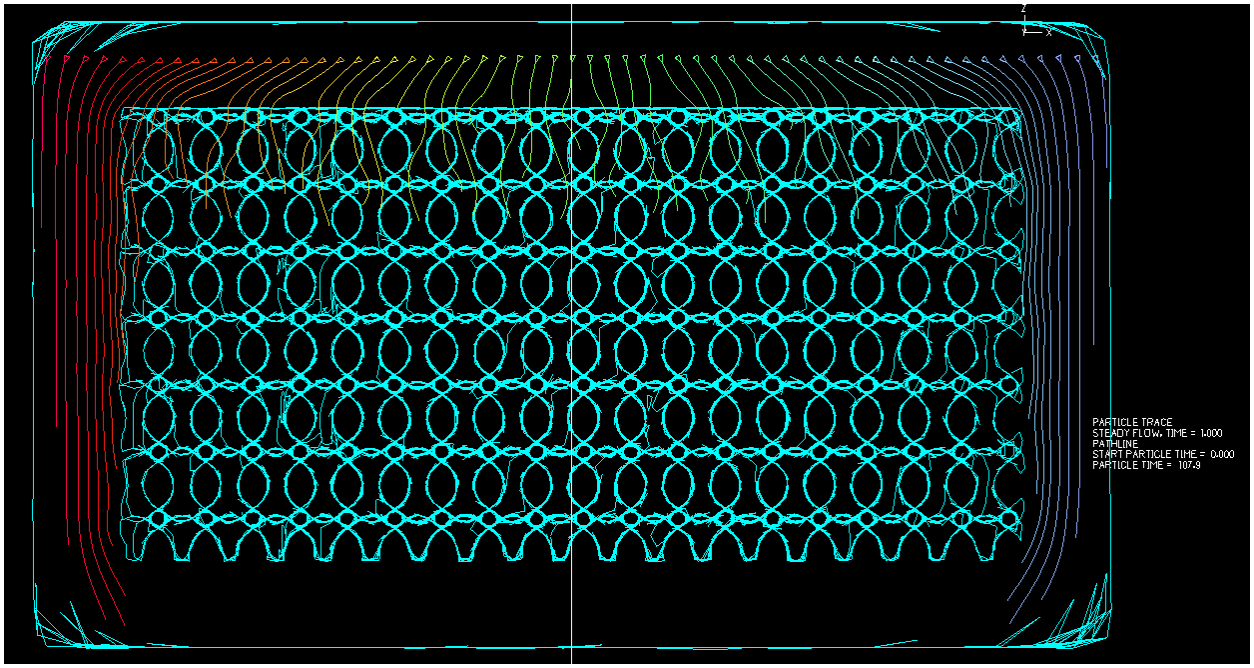


Figure 7: Non-perfusing flow that goes around, instead of through the scaffold.

Some interesting trends were observed in the scaffold diameter study. First, the overall shear stress increases as the scaffold diameter increases, which is visually represented in Figure 8. Additionally, the histograms (Figure 9) show a rightward movement of the curves with increasing scaffold diameters, showing the overall increase in shear stress on the scaffold. Interestingly, the spread of the distribution also seems to be increasing as the diameter increases; the standard

deviation generally increased from 0.19 mPa (diameter 10 mm model) to 0.22 mPa (diameter 10.49 mm model), and remained at 0.22 mPa (diameter 10.8 mm model). The percent differences between median shear stress values of each model were calculated and shown in Table 6. This study showed that changing the gap between the bioreactor chamber and the scaffold outer surface can significantly alter the shear stress distribution on the surface of the scaffold. Additionally, reducing this gap was shown to reduce the occurrence of non-perfusion flow around the scaffold.

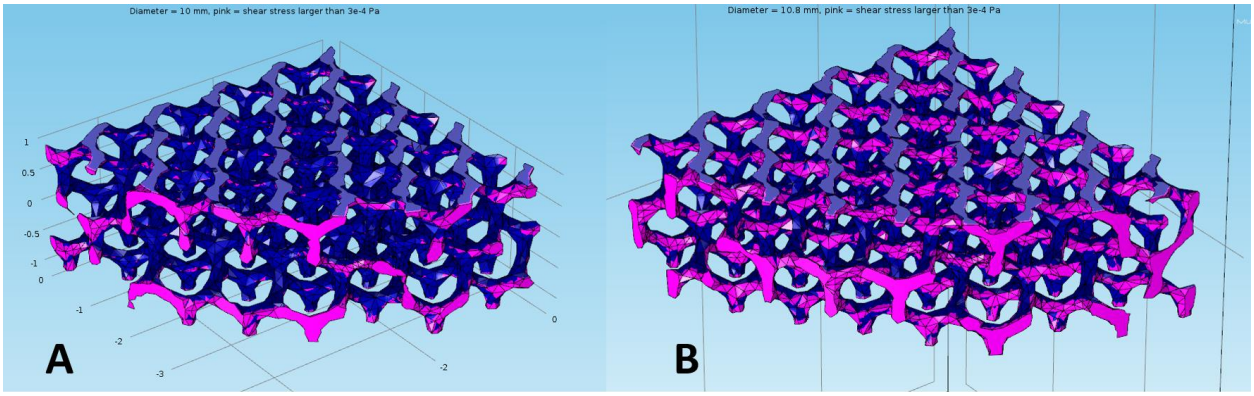


Figure 8: Visualization of the increase in shear stress as scaffold diameter increases. Regions with shear stress higher than 0.3 mPa are represented in pink in the scaffold with diameter 10 mm (A) and 10.8 mm (B). The larger diameter scaffold seems to have more areas of high shear stress distributed throughout the structure than the scaffold with diameter 10 mm. Non-perfusing shear stress is prevalent in the smaller diameter scaffold.

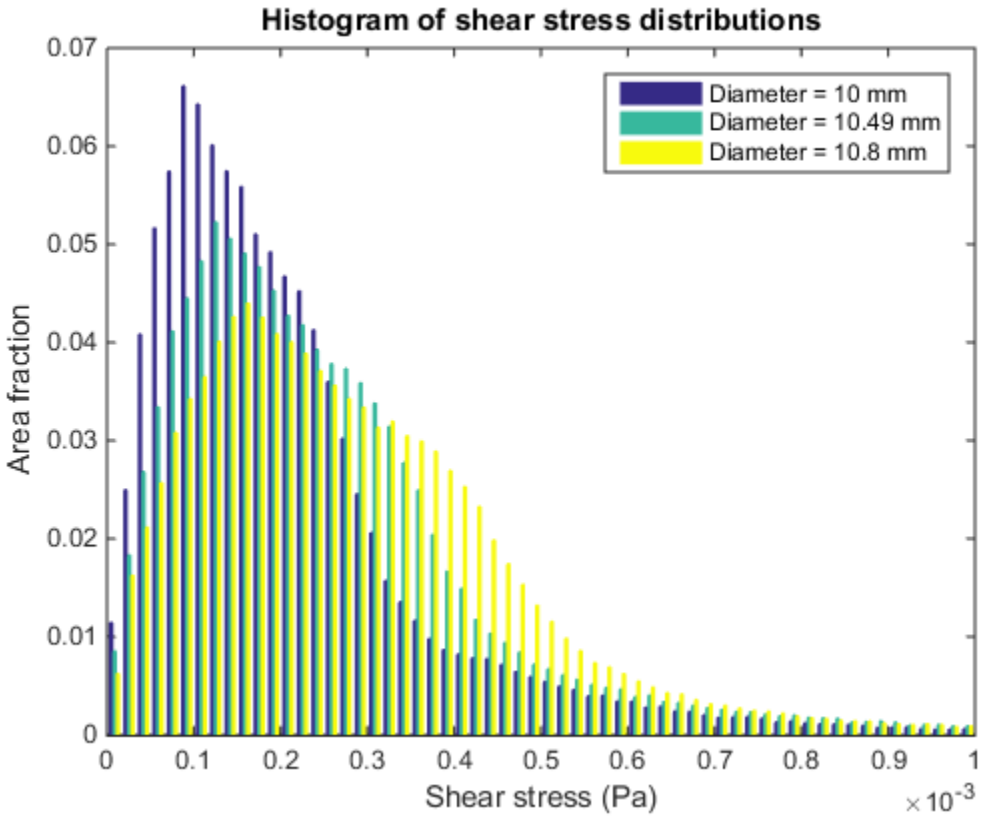


Figure 9: Histograms of shear stress distribution of scaffold with different diameters. There seems to be a right-ward movement of the curves as the scaffold diameter increases. As a result, the scaffold with diameter 10.8 has a higher population of shear stress larger than 0.3 mPa, which supports the observations made in Figure 8. Additionally, the curve seems to be more spread out as the diameter increases.

Table 6: Percent differences in median shear stresses of scaffolds with different diameters

| Comparison | 10 mm vs. 10.49 mm | 10 mm vs. 10.8 mm | 10.49 mm vs 10.8 mm |
|---|---|---|---|
| Percent Difference | 21.0% | 32.9% | 15.1% |

### 3.2.3 Strut size and pore size study

Average shear stresses on the surface of scaffolds with strut sizes from 0.125 mm to 0.3 mm and pore sizes from 0.3 mm to 0.7 mm are shown in Figure 5. Two prominent trends could be observed: first, average shear stress increases as the pore size increases; second, average shear stress decreases as strut size increases. However, when the pore size is small (0.3 – 0.4 mm), average shear stress does not seem to change with strut size. These behaviors might be due to the effects of non-perfusing flow: as the strut size increases or pore size deceases, the volume of perfusing fluid decreases. The pathway around the scaffold becomes more preferable while the flow through the scaffold's pores becomes more restricted. As a result, shear stress generally decreases with decreasing pore size or increasing strut size. These observations agreed with the data reported in Boschetti et al. (2006).

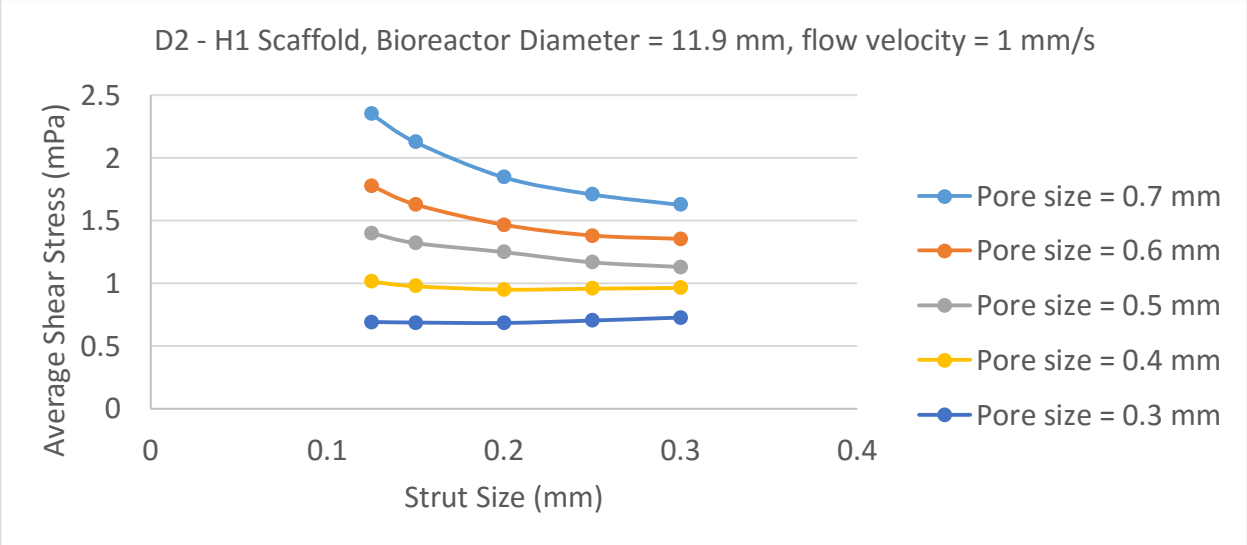


Figure 10: Average shear stress as a function of strut size and pore size. Generally, average shear stress increases with increasing pore size and decreases with increasing strut size.

As reflected in the percent differences (Table 5 and Table 6), large changes in shear stress occur when the overall size of the scaffold was modified. As a result, efforts to model reduced-sized scaffolds were ceased as these models would deviate significantly from the full-size scaffold. Additionally, the non-perfusing flow study showed that a gap of 0.95 mm creates a highly undesirable flow path around the scaffold. Considering the challenges in working with the D10 – H10 models, scaffolds with a diameter of 8 mm and height of 4 mm was 3D printed and modeled as the final working model. The new scaffold model still has a pore size of 0.7 mm and a strut size of 0.2 mm. This model, which is smaller than the original 10 mm x 10 mm scaffold, is small enough to be computationally analyzed. Since the scaffold is symmetrical in the sagittal planes, only a quarter of the cylindrical scaffold was analyzed, as previously described. With a new bioreactor chamber of diameter 8.66 mm, the new gap between the chamber wall and the scaffold's outer surface is 0.33 mm; the non-perfusing flow was eliminated in this new model.

### 3.3 Computational analysis of the new scaffold model

#### 3.3.1 Flow development study

The histograms of the shear stress distributions of D8 – H4 scaffolds with different entrance lengths were plotted on the same graph for comparison, as shown in Figure 10. Shear stress values lower than $10^{-11}$ Pa were removed from the histogram plot to provide a clear representation of the stress distribution.

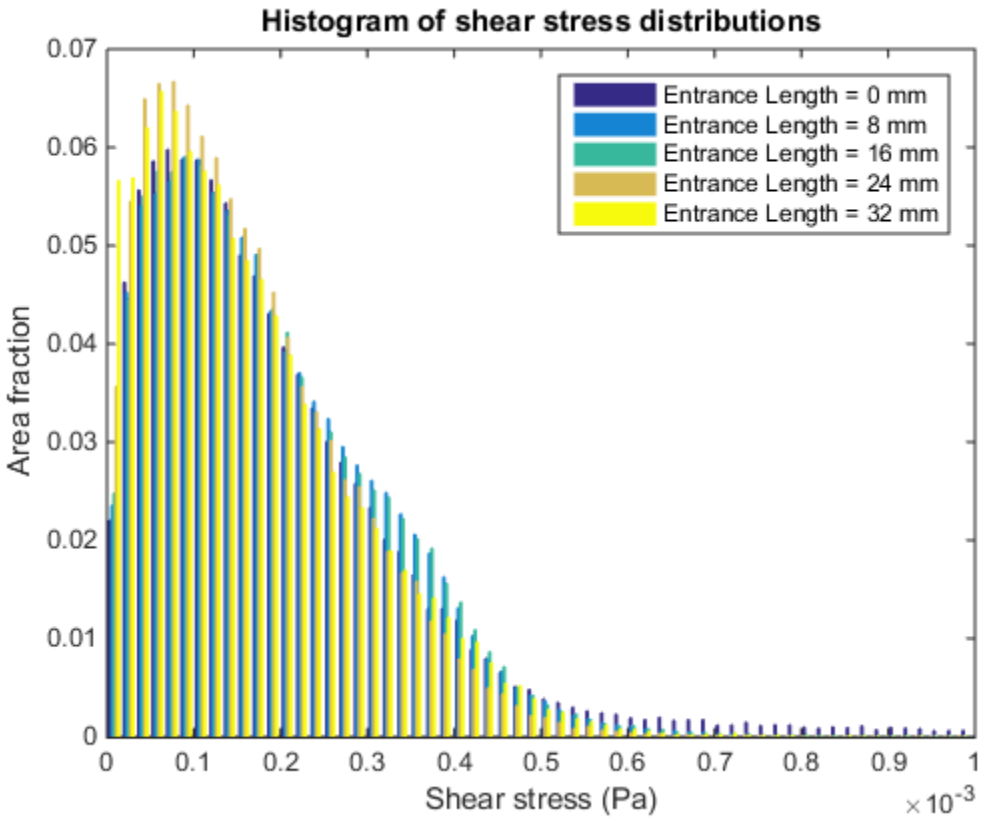


Figure 11: Shear stress distributions of models with different entrance lengths. Models with entrance lengths of 0, 8, and 16 mm deviated most from the 24 mm and 36 mm models near the shear stress regions of 0.05 – 0.15 mPa and 0.3 – 0.4 mPa.

Overall, the histograms exhibited a positive-skew distribution. The first three models (Entrance Lengths of = 0, 8, and 16 mm) seem to be most deviated from the "best" model (e.g. Entrance Length = 32 mm model, since it is the largest model made). Specifically, they have a higher population of shear stresses ranging from 0.3 to 0.4 mPa; additionally, they have higher populations of shear stress values smaller than $10^{-11}$ Pa (not shown). In contrast, the model with entrance length of 24 mm seems to closely follow the distribution of the best model. The percent differences between each model compared to the best model is shown in Table 7. The model with entrance length of 24 mm is most similar to the 32 mm, with an 8.9% difference. The model with

entrance length of 24 mm was chosen as it has a percentage difference less than 10% compared to the best model.

Table 7: Percent differences in median shear stresses in various entrance length models.

| Entrance Length | 0 mm | 8 mm | 16 mm | 24 mm |
|---|---|---|---|---|
| 32 mm | 36.5% | 47.0% | 45.5% | 8.9% |

### 3.3.2 Mesh convergence study

The histograms of shear stress distributions of scaffolds with increasing mesh densities showed similar trends (Figure 11). The number of elements of each mesh option is shown in Table 8. As an unknown glitch, COMSOL meshed the "Extra Coarse" model with the highest amount of elements, which is contradictory to what was expected. Regardless, the "Coarse" model is the only model with a percent difference less than 10%, therefore, was chosen for subsequent CFD studies (Table 9).

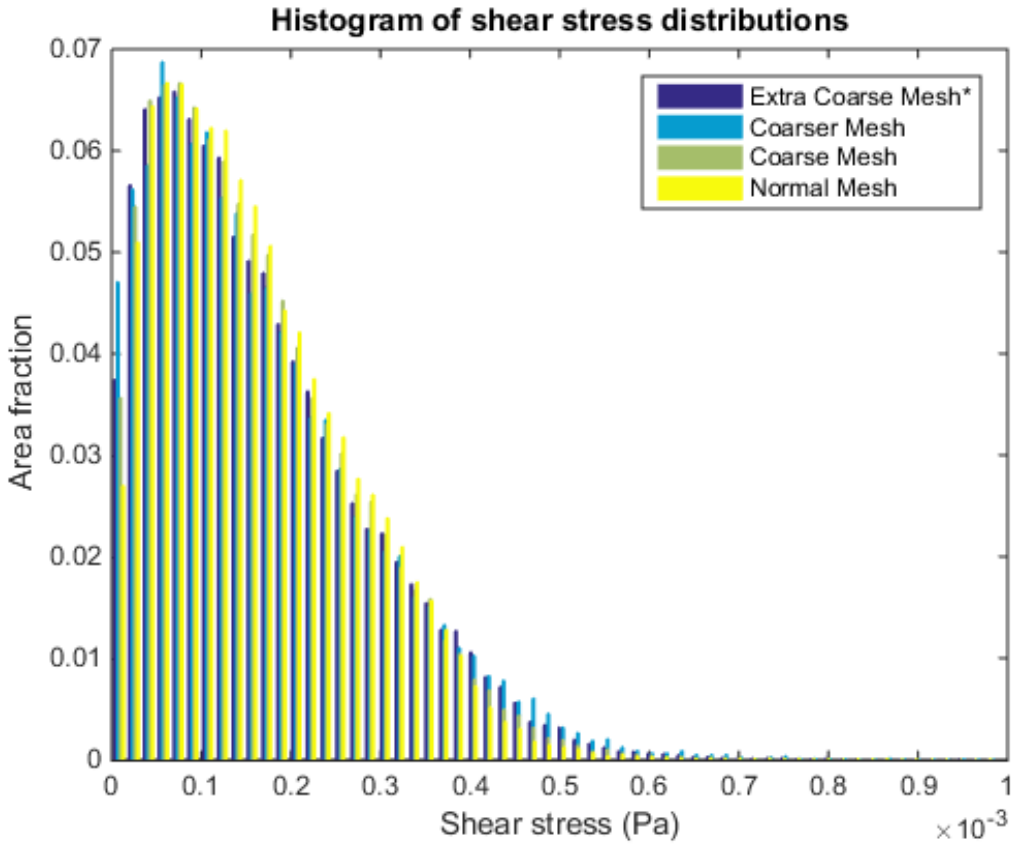


Figure 12: Shear stress distributions of models with different mesh densities.

Table 8: Number of elements of each mesh density. For an unknown reason, "Extra Coarse" mesh has the largest number of elements.

| Mesh Type | Normal | Coarse | Coarser | Extra Coarse* |
|---|---|---|---|---|
| Number of Elements | 165656 | 154629 | 151707 | 176300 |

Table 9: Percent difference of mean shear stresses of various mesh densities. "Coarse" mesh is closest to the "Normal" mesh, with a 9.9% different in median shear stress.

| Mesh Density Type | Extra Coarse Mesh | Coarser Mesh | Coarse Mesh |
|---|---|---|---|
| Normal Mesh | 14.0% | 19.4% | 9.9% |

### 3.3.3 Flow velocity study

The mean shear stress values are linearly related to the inlet velocity, as shown in Figure 12. This relationship was expected because the perfusing medium is water, which is a Newtonian liquid. An equation that describes shear stress as a function of flow velocity was given by:

$$\tau = 0.007 \times u$$

Where $\tau$ is the shear stress on the surface of the scaffold, and $u$ is the inlet velocity. This equation allows for the easy interconversion of shear stress and inlet velocity in our particular CFD model, which facilitates the use of calculated shear stress values found from the meta-analysis study with known cellular behaviors. Consequently, desirable shear stresses on the scaffolds can be achieved by using appropriate flow rates derived from this equation. The flow rates needed to obtain the target shear stress values are shown in Table 10, with the hypothesis for each shear stress listed.

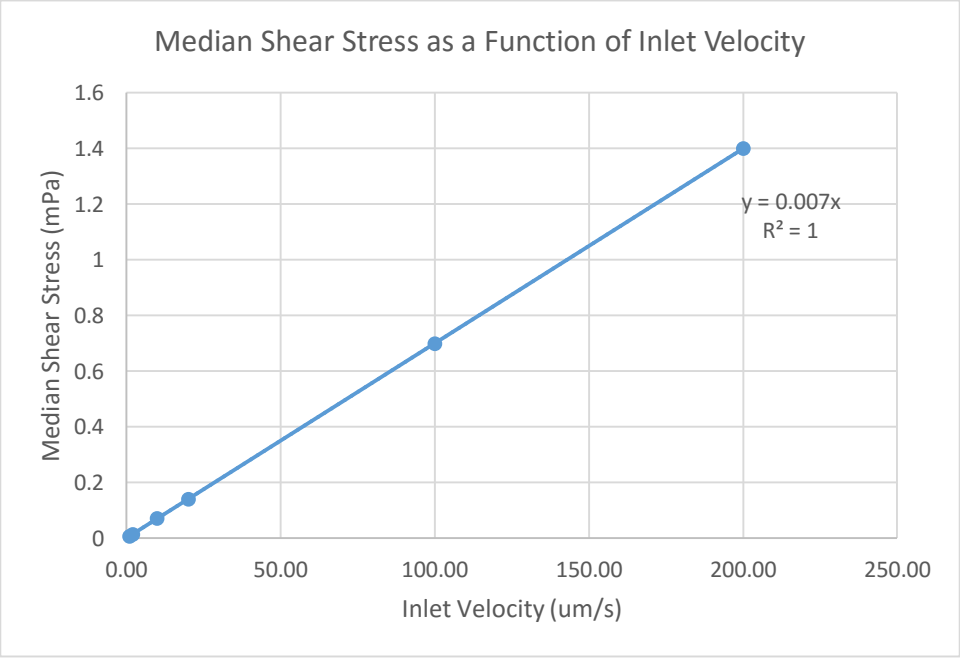


Figure 13: The linear relationship between shear stress and inlet flow velocity.

Table 10: Target shear stresses and flow rates needed.

| Shear Stress (mPa) | Flow Velocity (um/s) | Flow Rate (ml/hour) | Hypothesis |
|---|---|---|---|
| 0.025 | 3.571 | 0.757 | Improved mass transport |
| 0.250 | 35.714 | 7.573 | Improved proliferation via shear stress |
| 2.500 | 357.143 | 75.730 | Improved proliferation via shear stress |
| 25.000 | 3571.429 | 757.304 | Cell detachment |

### 3.4 Cell proliferation study using the perfusing bioreactor system

A cell proliferation study using flow rates of 0.757 ml/hour and 75.730 ml/hour was initiated. After the scaffolds have been placed into the bioreactor chambers, the well plate used for seeding scaffolds was observed under the microscope. Unfortunately, many cells remained in the well plate, suggesting that cells did not sufficiently attached to the surface of the scaffolds for the experiment to continue. Consequently, the study was aborted.

Additionally, the perfusion bioreactors also showed undesirable characteristics (Figure 13). Although carefully primed, there was still air bubbles collecting inside the bioreactor chambers. Some scaffolds were pushed up to the top of the chamber by the air bubbles, exposing the scaffolds to air. Moreover, some scaffolds were stuck at an angle instead of lying flat on the bottoms of the bioreactor chambers.

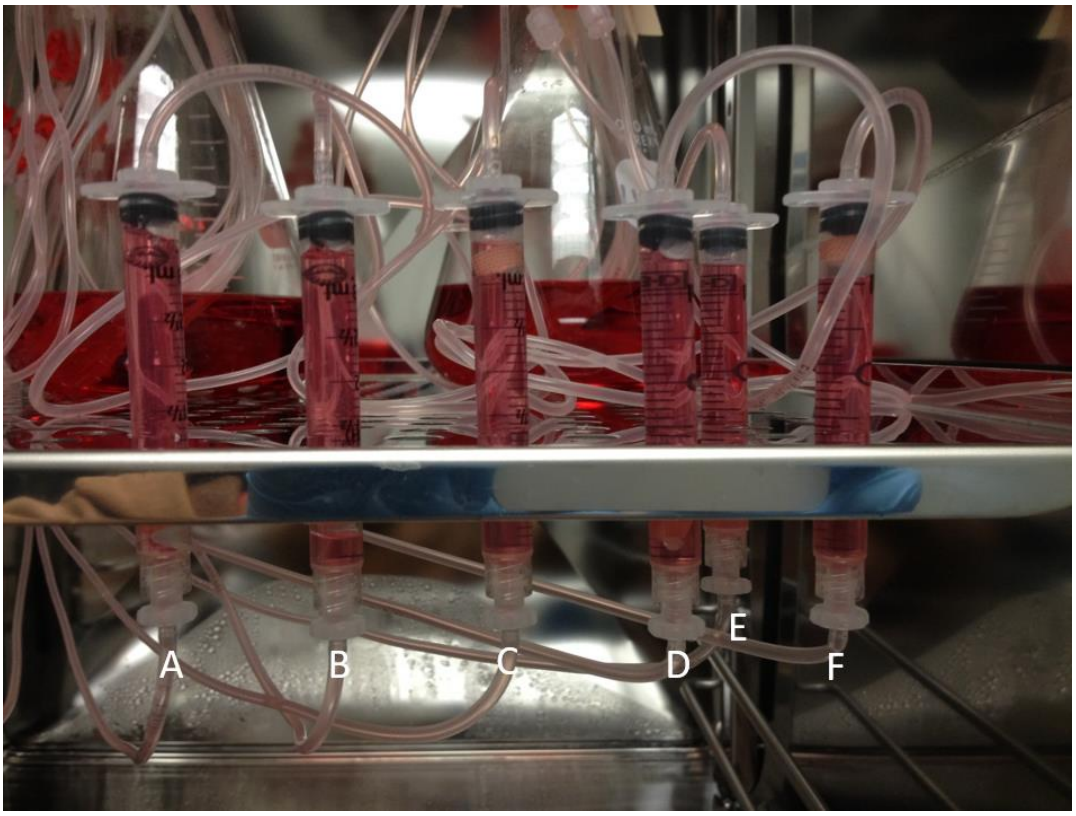


Figure 14: Visualization of the perfusion bioreactors. All scaffolds had air bubbles trapped underneath. In particular, scaffolds A and B seemed to be floating on top of big air bubbles. Scaffold C floated to the top of the chamber. Scaffold D and E were at an angle near the bottom. Scaffold F floated on the top of the bioreactor chamber and fully exposed to air.

## CHAPTER 4: CONCLUSION AND FUTURE WORK

In this study, we quantified the shear stress distributions of scaffolds with Gyroid pore architecture in the perfusion bioreactors using a computational fluid dynamics method. The computer simulations identified a fault in our perfusion system, in which the perfusing fluid was mostly going around instead of through the scaffold. This happened because there was a big gap between the inner wall of the bioreactor chamber and the outer surface of the scaffold. This gap was reduced in the subsequent model; as a result, more fluid was able to perfuse through the scaffold with the new model.

Through a simple engineering model, an analytical equation was derived to relate flow rate to shear stress. The analytical equation provided similar results to the shear stresses reported in the literature and also to those obtained from the computer simulations done in this project. With this simple yet useful equation, shear stresses were estimated from previous publications that did not report these values. Consequently, a table of shear stresses with their effects on cellular behaviors was compiled and presented.

The perfusion system is perhaps the component that requires the most attention. The scaffolds have been observed to be floating in the chambers while the study was running, instead of lying flat on the bottom of the chambers. Some scaffolds were stuck at an angle, changing the calculated flow paths and opening gaps between the scaffolds and the bioreactor, which could cause non-perfusing flow. In subsequent studies, thin rubber rings will be used to hold the scaffolds in place at the bottoms of the chambers, preventing the scaffolds to float or rotate to an undesirable angle.

Although the perfusing bioreactors were carefully primed, air bubbles were still collected inside the bioreactor chambers after a couple days. This might be because when the scaffolds were

transferred from the seeding well plate into the bioreactor chambers, media might have seeped out of the scaffolds, allowing small pockets of air to collect inside the pores of the scaffolds. In the future, a vacuum chamber should be used after the scaffolds are placed inside the bioreactors to ensure that scaffolds are fully submerged in media. Additionally, degassing vacuum pumps might be installed in the perfusing system so all air bubbles will be eliminated *in situ* as the experiment progresses.

Additionally, although the perfusing bioreactors can be quickly and inexpensively built and maintained, they do not provide the capability for anatomically shaped scaffolds since the gap between the chamber wall and scaffold's outer surface needs to be minimized. This problem might be overcome by using a polydimethylsiloxane (PDMS) mold that tightly holds the anatomically shaped scaffolds in place inside the bioreactor chamber. All fluid that goes through the PDMS mold will also perfuse through the scaffold inside, ensuring that all regions of the scaffold will have access to nutrients.

By ensuring to use ultra-low attachment well plates and allowing the L929 cells to seed on scaffolds overnight, we would like to see more cells attach to the surface of the scaffolds in future studies. Through fluid-induced shear stress, the perfusing bioreactors might provide a well-regulated method to improve the growth and differentiation of stem cells within the scaffold. With a combination of differentiation factors in the perfusing medium and an appropriate level of shear stresses, the perfusing bioreactors allow for the culturing of practical bone grafts with clinically relevant sizes and robust functionalities for bone tissue engineering applications.

BIBLIOGRAPHY

Atala A, Yoo J. Essentials of 3D Biofabrication and Translation, 1st ed.; Academic Press: Waltham, MA, 2015.

Bancroft GN, Sikavitsast VI, van den Dolder J, Sheffield TL, Ambrose CG, Jansen JA, Mikos AG. Fluid flow increases mineralized matrix deposition in 3D perfusion culture of marrow stromal osteoblasts in a dose-dependent manner. Proceedings of the National Academy of Sciences of the United States of America 2002 99:12600-12605.

Bancroft GN, Sikavitsas VI, Mikos AG. Technical Note: Design of a flow perfusion bioreactor system for bone tissue-engineering applications. Tissue Engineering 2004 (9:3):549-554.

Boschetti F, Raimondi MT, Migliavacca F, Dubini G. Prediction of the micro-fluid dynamic environment imposed to three-dimensional engineered cell systems in bioreactors. Journal of Biomechanics 2006 39:418-425.

Cartmell SH, Porter BD, Garcia AJ, Guldberg RE. Effects of medium perfusion rate on cell-Seeded Three-Dimentional Bone Constructs *in Vitro*. Tissue engineering 2003 9(6): 1197-1203.

Cioffi M, Boschetti F, Raimondi MT, Dubini G. Modeling evaluation of the fluid-dynamic microenvironment in tissue-engineered constructs: a micro-CT based model. Biotechnology and Bioengineering 2006 93:500-510.

Dean D, Min K-J, Bond A. Computer aided design of large format prefabricated cranial plates. Journal of Craniofacial Surgery 2003, 14(6):819-832.

Fisher JP, Dean D, Mikos AG. Photocrosslinking characteristics and mechanical properties of diethyl fumarate/poly(propylene fumarate) biomaterials. Biomaterials 2002, 23(22):4333-4343.

Glowacki J, Mizuno S, Greenberge JS. Perfusion enhances functions of bone marrow stromal cells in three-dimensional culture. Cell Transplantation 1998 7:319-326.

Goldstein AS, Juarez TM, Helmke CD, Gustin MC, Mikos AG. Effect of convection on osteoblastic cell growth and function in biodegradable polymer foam scaffolds. Biomaterials 2001 22(11):1279-1288.

Grayson WL, Bhumiratana S, Cannizzaro C, Chao GP, Lennon D, Caplan AI, Vunjak-Novakovic G. Effect of initial seeding density and fluid perfusion rate on formation of tissue-engineered bone. Tissue Eng A 2008 14(11):1809-1820.

Grayson WL, Frohlich M, Yeager K, Bhumiratana S, Cannizarro C, Chan ME, Wan QL, Liu X, Guo XE, Vunjak-Novakovic G. Engineering anatomically-shaped human bone grafts. Proc Natl Acad Sci USA 2010 107(8):3299-3304.

Grayson WL, Marolt D, Bhumiratana S, Frohlich M, Guo XE, Vunjak-Novakovic G. Optimizing the medium perfusion rate in bone tissue engineering bioreactors. Biotechnology and Bioengineering 2011 108(5):1159-1170.

Holy CE, Shoichet MS, Davies JE. Engineering three-dimensional bone tissue in vitro using biodegradable scaffolds: Investigating initial cell-seeding density and culture period. J Biomed Mater Res 200 51(3):376-382.

Ishaug, SL, Crane GM, Miller MJ, Yasko AW, Yaszemski MJ, Mikos AG. Bone formation by three-dimentional stromal osteoblast culture in biodegradable polymer scaffolds. J Biomed Mater Res 1997 36(1):17-28.

Ishaul-Riley SL, Crane-Kruger GM, Yaszemski MJ, Mikos AG. Three-dimensional culture of rat calvarial osteoblasts in porous biodegradable polymers. Biomaterials 1998 19(15):1405-1412.

Jarman-Smith M, Bodamyali T, Stevens C, Howell JA, Horrocks M, Chaudhuri JB. Human fibroblast culture on a crosslinked dermal porcine collagen matrix. Biochem Eng J 2004 20(2-3):217-222.

Jungreuthmayer C, Donahue SW, Jaasma MJ, Al-Munajjed AA, Zanghellini J, Kelly DJ, O'Brien FJ. A comparative study of shear stresses in collagen-glycosaminoglycan and calcium phosphate scaffolds in bone tissue-engineering bioreactors. Tissue Engineering Part A 2009 15:1141-1149.

Korin N, Bransky A, Dinnar U, Levenberg S. A parametric study of human fibroblasts culture in a microchannel bioreactor. Lab Chip 2007 7(5):611-617.

Langer R, Vacanti J. Tissue Engineering. Science 1993 260(5110):920-926

Lee JW, Kang KS, Lee SH, Kim JU, Lee BK, Cho DW. Bone regeneration using a microstereolithography-produced customized poly(propylene fumarate)/diethyl fumarate photopolymer 3D scaffold incorporating BMP-2 loaded PLGA microspheres. Biomaterials 2011, 32(3):744-752.

Liu D, Chua C-K, Leong K-F. Impact of short-term perfusion on cell retention for 3D bioconstructs development. J Biomed Mater Res Part A 2013 101A:647-652.

Luo Y, Dolder CK, Walker JM, Mishra R, Dean D, Becker ML. Synthesis and Biological Evaluation of Well-Defined Poly(propylene fumarate) Oligomers and Their Use in 3D Printed Scaffolds. Biomacromolecules 2016 17(2):690-697.

Maes F, Van Ransbeeck P, Van Oosterwyck H, Verdonck P. Modeling fluid flow through irregular scaffolds for perfusion bioreactors. Biotechnology and Bioengineering 2009 103:621-630.

Maes F, Claessens T, Moesen M, Van Oosterwyck H, Van Ransbeeck P, Verdonck P. Computational models for wall shear stress estimation in scaffolds: a comparative study of two complete geometries. Journal of Biomechanics 2012 45:1586-1592.

Mahmoudifar N, Doran PM. Chondrogenic differentiation of human adipose-derived stem cells in polyglycolic acid mesh scaffolds under dynamic culture conditions. Biomaterials 2010 31:3858-3867.

Martins AM, Saraf A, Sousa RA, Alves CM, Mikos AG, Kasper FK, Reis RL. Combination of enzymes and flow perfusion conditions improves osteogenic differentiation of bone marrow stromal cells cultured upon starch/poly(epsilon-caprolactone) fiber meshes. J Biomed Mater Res Part A 2010 94A:1061-1069.

Marolt D, Augst A, Freed LE, Vepari C, Fajardo R, Patel N, Gray M, Farley M, Kaplan D, Vunjak-Novakovic G. Bone and cartilage tissue constructs grown using human bone marrow stromal cells, silk scaffolds and rotating bioreactors. Biomaterials 2006 27(36):6138-6149.

Meinel L, Karageorgiou V, Fajardo R, Snyder B, Shinde-Patil V, Zichner L, Kaplan D, Langer R, Vunjak-Novakovic G. Bone tissue engineering using human mesenchymal stem cells: Effects of scaffold material and medium flow. Ann Biomed Eng 2004a (31(1):112-122.

Michielsen K, Stavenga DG. Gyroid cuticular structures in butterfly wing scales: biological photonic crystals. J R Soc Interface 2008 5(18):85-94.

Ratner BD, Hoffman AS, Schoen FJ, Lemons JE. Biomaterials Science: An Introduction to Materials in Medicine, 2nd ed. Elsevier Academic Press: New York, 2004.

Sandino C, Planell, JA, Lacroix D. A finite element study of mechanical stimuli in scaffolds for bone tissue engineering. Journal of Biomechanics 2008 41:1005-1014.

Song MJ, Dean D, Knothe-Tate ML. Mechanical modulation of nascent stem cell lineage commitment in tissue engineering scaffolds. Biomaterials 2013 34(23):5766-5775.

Sikavitsas VI, Bancroft GN, Mikos AG. Formation of three-dimensional cell/polymer constructs for bone tissue engineering in a spinner flast and a rotating wall vessel bioreactor. J Biomed Mater Res 2002 62(1):136-148.

Temenoff JS, Mikos AG. Injectable biodegradable materials for orthopedic tissue engineering. Biomaterials 2000, 21(23):2405-2412.

Wang CF, Wang Z, Li AM, Bai F, Lu JX, Xu Sl, Li DC. Repair of segmental bone-defect of goat's tibia using a dynamic perfusion culture tissue engineering bone. J Biomed Mater Res Part A 2010 92A:1145-1153.

Wang S, Lu L, Yaszemski MJ. Bone-Tissue-Engineering Material Poly(propylene fumarate): Correlation between Molecular Weight, Chain Dimensions, and Physical Properties. Biomacromolecules 2006, 7(6):1976 – 1982.

APPENDIX A: THE ENGINEERING MODEL AND THE DERIVATION OF AN ANALYTICAL SOLUTION

$$(\pi r^2)P + (2\pi r dx)\tau = (\pi r^2)(P + dP)$$
$$(2\pi r dx)\tau = (\pi r^2)dP$$
$$\tau = \frac{r}{2}\frac{dP}{dx}$$

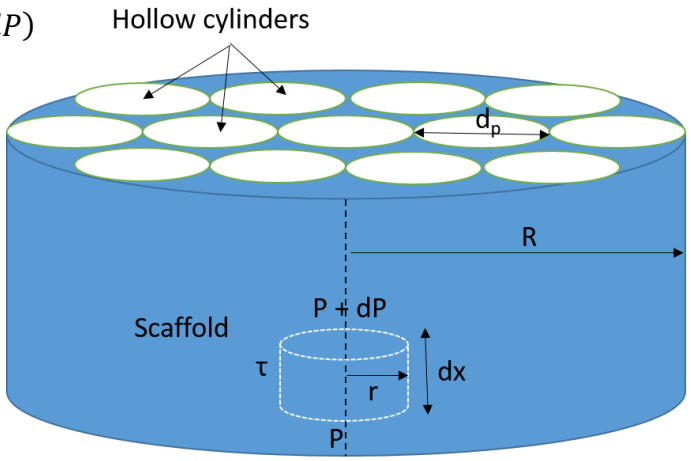


*Definition of fluid*:

$$\tau = \mu\frac{du}{dr}$$
$$\frac{r}{2}\frac{dP}{dx} = \mu\frac{du}{dr}$$
$$du = \frac{1}{2\mu}\frac{dP}{dx}r dr$$
$$\int du = \int \frac{1}{2\mu}\frac{dP}{dx}r dr$$
$$U(r) = \frac{1}{2\mu}\frac{dP}{dx}\frac{r^2}{2} + C$$

*No slip boundary condition*:

$$U(R) = 0$$
$$U(r) = \frac{1}{4\mu}\frac{dP}{dx}(r^2 - R^2)$$

*Flow rate*:

$$Q = \int U(r)dA = \int_0^R \underbrace{\frac{1}{4\mu}\frac{dP}{dx}(r^2 - R^2)}_{U(r)}\underbrace{2\pi r dr}_{dA}$$
$$Q = \frac{-\pi R^4}{8\mu}\frac{dP}{dx}\ (Hagen - Poiseulle\ Flow)$$

*Since*:

$$\tau = \frac{r}{2}\frac{dP}{dx}$$
$$Q = \frac{-\pi R^3}{4\mu}\tau_{wall}$$
$$\tau_{wall} = \frac{4\mu Q}{\pi R^3}$$

$$\boxed{\tau_{wall} = \frac{8\mu Q}{d_p \pi R^2}}$$

APPENDIX B: BUILDING THE BIOREACTOR SYSTEM

1. Remove the metal tray out of the incubator, spray with ethanol before putting it into the BSC.
2. Obtain the bag with sterile bioreactor chambers.
3. Obtain the bag with sterile lines between bioreactors and incubator plug.
4. Obtain the bag with the sterile incubator plug.
5. Thread the connecting lines through the hole in the back of the tray.
6. Insert the bioreactor chambers into the metal tray.
7. Connect the connecting lines between the chambers and the plug.
8. Obtain the bags with the sterile reservoir plugs.
9. Obtain the bags with the sterile black gaskets.
10. Insert the black gaskets into the ends of the plug lines.
11. Insert the black gaskets into the chambers.
12. Obtain the sterile empty medium reservoirs.
13. Obtain the complete DMEM.
14. Fill the reservoirs, each with 500 ml of medium.
15. Connect the plugs to the reservoirs.
16. Obtain a sterile 60-ml syringe and appropriate connectors.
17. Fill the syringe with Complete DMEM.
18. Infuse the fluid from the incubator plug end, through the bioreactor chambers, into the reservoirs.
19. Close the clip after each line is primed.
20. Obtain the well plate of scaffolds with cells.
21. Obtain sterile forceps.

22. Obtain the sterile rubber O rings.
23. Clip the lines above the bioreactor chambers.
24. Unplug the black gaskets, transfer the scaffolds into the chambers, push the O rings and the scaffolds down to the bottoms of the chambers.
25. Use the vacuum chamber to ensure that all air bubbles are removed from the scaffolds.
26. Refill the bioreactor with DMEM if needed.
27. Plug the black gaskets back into the chambers.
28. Unclip the lines.
29. Spray the entire tray with ethanol before inserting it back into the incubator.
30. Thread the incubator plug through the hole behind the incubator.
31. Connect the lines between the syringe pumps and the incubator plug, be careful not to break sterility.
32. Set up the syringe pumps as desired.

Appendix C: MATLAB CODES

```
%Archie Tram Honor's Thesis - Spring 2016
%Scaffold Height Study
clc
close all
clear all
load('cleandata.mat')

mediandata = [median(H1p5) median(H2) median(H3)];

h1p5vsh3 = abs(mediandata(1) - mediandata(3))* 100/(mediandata(3));
h2vsh3 = abs(mediandata(2) - mediandata(3))* 100/(mediandata(3));
h1p5vsh2 = abs(mediandata(1) - mediandata(2))* 100/(mediandata(2));

load('cleandata_truncated.mat')
[count1, data1] = hist(H1p5,60);
[count2, data2] = hist(H2,60);
[count3, data3] = hist(H3,60);

normalcount1 = count1 ./sum(count1);
normalcount2 = count2 ./sum(count2);
normalcount3 = count3 ./sum(count3);
```

```
bar([data1;data2;data3]',[normalcount1;normalcount2;normalcount3]','grouped')
title('Histogram of shear stress distributions')
ylabel('Area fraction')
xlabel('Shear stress (Pa)')
legend('Height = 1.5 mm','Height = 2 mm', 'Height = 3 mm')

%Archie Tram Honor's Thesis - Spring 2016
%Scaffold Diameter Study
clc
close all
clear all
load('cleandata.mat')

mediandata = [median(D10) median(D10p49) median(D10p8)];
stds = [std(D10) std(D10p49) std(D10p8)];


D10_v_D10p8 = abs(mediandata(1) - mediandata(3))* 100/(mediandata(3));
D10p49_v_D10p8 = abs(mediandata(2) - mediandata(3))* 100/(mediandata(3));
D10_v_D10p49 = abs(mediandata(1) - mediandata(2))* 100/(mediandata(2));

load('cleandata_truncated.mat')
```

```
[count1, data1] = hist(D10,60);
[count2, data2] = hist(D10p49,60);
[count3, data3] = hist(D10p8,60);

normalcount1 = count1 ./sum(count1);
normalcount2 = count2 ./sum(count2);
normalcount3 = count3 ./sum(count3);

bar([data1;data2;data3]',[normalcount1;normalcount2;normalcount3]','grouped')
title('Histogram of shear stress distributions')
ylabel('Area fraction')
xlabel('Shear stress (Pa)')
legend('Diamter = 10 mm','Diamter = 10.49 mm', 'Diamter = 10.8 mm')

%Archie Tram Honor's Thesis - Spring 2016
%Flow Development Study
clc
close all
clear all
load('cleandata.mat')

mediandata = [median(flowdev0) median(flowdev2) median(flowdev4) median(flowdev6)
median(flowdev8)];
```

```
percent_entrance0 = abs(mediandata(1) - mediandata(5))* 100/(mediandata(5));

percent_entrance2 = abs(mediandata(2) - mediandata(5))* 100/(mediandata(5));

percent_entrance4 = abs(mediandata(3) - mediandata(5))* 100/(mediandata(5));

percent_entrance6 = abs(mediandata(4) - mediandata(5))* 100/(mediandata(5));


load('cleandata_truncated1.mat')

[count1, data1] = hist(flowdev0,60);

[count2, data2] = hist(flowdev2,60);

[count3, data3] = hist(flowdev4,60);

[count4, data4] = hist(flowdev6,60);

[count5, data5] = hist(flowdev8,60);


normalcount1 = count1 ./sum(count1);

normalcount2 = count2 ./sum(count2);

normalcount3 = count3 ./sum(count3);

normalcount4 = count4 ./sum(count4);

normalcount5 = count5 ./sum(count5);


bar([data1;data2;data3;data4;data5]',[normalcount1;normalcount2;normalcount3;normalcount4;n

ormalcount5]','grouped')

title('Histogram of shear stress distributions')

ylabel('Area fraction')
```

```
xlabel('Shear stress (Pa)')
legend('Entrance Length = 0 mm','Entrance Length = 8 mm', 'Entrance Length = 16 mm', 'Entrance
Length = 24 mm', 'Entrance Length = 32 mm')

%Archie Tram Honor's Thesis - Spring 2016
%Mesh Convergence Study
clc
close all
clear all
load('cleandata.mat')

mediandata = [median(Normal) median(Coarse) median(Coarser) median(ExtraCoarse)];

percent_extracoarse = abs(median(ExtraCoarse) - median(Normal))* 100/(median(Normal));
percent_coarser = abs(median(Coarser) - median(Normal))* 100/(median(Normal));
percent_coarse = abs(median(Coarse) - median(Normal))* 100/(median(Normal));


load('cleandata_truncated.mat')
[count1, data1] = hist(ExtraCoarse,60);
[count2, data2] = hist(Coarser,60);
[count3, data3] = hist(Coarse,60);
[count4, data4] = hist(Normal,60);
```

```
normalcount1 = count1 ./sum(count1);

normalcount2 = count2 ./sum(count2);

normalcount3 = count3 ./sum(count3);

normalcount4 = count4 ./sum(count4);



bar([data1;data2;data3;data4]',[normalcount1;normalcount2;normalcount3;normalcount4]','group
ed')

title('Histogram of shear stress distributions')

ylabel('Area fraction')

xlabel('Shear stress (Pa)')

legend('Extra Coarse Mesh*','Coarser Mesh', 'Coarse Mesh', 'Normal Mesh')
```